JOURNAL OF GUIDANCE, CONTROL, AND DYNAMICS
Vol. 20, No. 6, November–December 1997

Adaptive Control of Aeroelastic Instabilities in Transonic Flow and Its Scaling

P. P. Friedmann,* D. Guillot,† and E. Presente‡
University of California, Los Angeles, Los Angeles, California 90095-1597

A two-dimensional aeroservoelastic study in the time domain is described. The model, based on exact inviscid aerodynamics, correctly represents the large amplitude motions and the associated strong shock dynamics in the transonic regime. The aeroservoelastic system consists of a two-degree-of-freedom airfoil with a trailing-edge control surface. Active flutter suppression in the presence of nonlinear aeroelastic phenomena is achieved using first-order actuator dynamics and a digital adaptive controller. A relation between actuator dynamics and limits on the flap deflection angle to guarantee the effectiveness of the adaptive controller is illustrated by the results. Hinge moment calculations and power requirements for flutter suppression are also carried out. Aeroelastic scaling requirements for the governing parameters, including actuator moment and control power, are established.

Nomenclature

$[A_P]$, $\{B_P\}$, $[C_P]$	= aeroservoelastic system matrices
a_h	= nondimensional elastic axis location measured from midchord
a_i	= autoregressive (AR) coefficient
a_∞	= freestream sound velocity
b	= airfoil semichord
b_i	= moving average (MA) coefficient
C_h	= hinge moment coefficient
C_l, C_m	= lift and moment coefficients about the elastic axis, respectively
C_P	= pressure coefficient, $2(p - p_\infty)/\rho V^2$
$C(k)$	= Theodorsen's lift deficiency function
c	= chord
c_β	= nondimensional flap hinge axis location measured from midchord
$\{\boldsymbol{D}_i\}$	= artificial dissipation vector at node i
$\{\boldsymbol{G}\}_k$	= controller gain vector at time kT_e
H, $\bar{H}$	= hinge moment, and nondimensional hinge moment per unit span
h	= plunge displacement
I_α	= moment of inertia of the airfoil with flap in neutral position, about the elastic axis
I_β	= flap moment of inertia about the hinge axis
J	= performance index
K_h, K_α, K_β	= spring constants, restraining bending, torsion, and flap rotation
k	= reduced frequency, $\omega b/V$
L	= lift per unit span
$\{\boldsymbol{L}\}_k$	= estimator gain vector at time kT_e
L_m, L_w	= length for model and full-scale configuration
M	= Mach number
$[M]$, $[K]$	= mass and stiffness matrices for the three-degree-of-freedom airfoil section
M_m, M_w	= mass for model and full-scale configuration, respectively
M_α	= pitch moment per unit span
m	= airfoil mass per unit span
N_n	= number of nodes in the mesh surrounding the airfoil
n_L, n_M, n_T	= scaling factors for length, mass, and time
P, $\bar{P}$	= power and nondimensional power, respectively, per unit span
$[P]$	= steady-state Riccati matrix
$\bar{P}_{\text{av}}$	= average nondimensional power
$[P]_k$	= Riccati matrix at time kT_e
p	= pressure
$[Q]$	= positive semidefinite symmetric matrix
$\{\boldsymbol{Q}_i\}$	= flux vector at node i
r_w	= positive weighting coefficient
r_α	= radius of gyration of the airfoil about its elastic axis, $[I_\alpha/(mb^2)]^{1/2}$
r_β	= radius of gyration of the flap about its hinge axis, $[I_\beta/(mb^2)]^{1/2}$
S_α	= static moment of the airfoil with flap in neutral position, about the elastic axis
S_β	= flap static moment, about the hinge axis
T_e	= sampling time step for parameter estimator
T_m, T_w	= time for model and full-scale configuration, respectively
$T_1, \ldots, T_{19}$	= constants used in Theodorsen-type aerodynamics
t	= time
$\bar{t}$	= nondimensional time, $(\omega_\alpha t)/2\pi$
$\bar{t}_1$, $\bar{t}_2$	= nondimensional times used in power calculation
$\bar{U}$	= nondimensional speed, $V/(b\omega_\alpha)$
$[U]$	= eigenmatrix of order $n \times m$
V	= freestream velocity
$[V]_k$	= covariance matrix at time kT_e
$\{\boldsymbol{w}_i\}$	= flow vector at node i
$\{\boldsymbol{w}_{\text{ST}}\}$	= structural state vector, $[\{q\}^T, \{\dot{q}\}^T]^T$
$\{\boldsymbol{x}_p\}$	= state vector of the estimated deterministic ARMA model
x_α	= nondimensional static moment of the airfoil with flap in neutral position, about the elastic axis, $S_\alpha/(mb)$; also static unbalance, nondimensionalized with respect to the semichord b
x_β	= nondimensional flap static moment about the hinge axis, $S_\beta/(mb)$
y	= output of the ARMA model
y_k	= wing response at sensor, at time kT_e
α, α_0	= airfoil angle of attack and pitch amplitude
β, β_0	= flap deflection angle and amplitude of flap deflection, respectively
$\beta_{\max}$	= maximum commanded flap angle
γ	= ratio of specific heat coefficients

Presented as Paper 97-0581 at the AIAA 35th Aerospace Sciences Meeting, Reno, NV, Jan. 6–9, 1997; received Jan. 27, 1997; revision received June 9, 1997; accepted for publication June 9, 1997.

*Professor, Mechanical and Aerospace Engineering Department. Fellow AIAA.

†Visiting Scholar, Mechanical and Aerospace Engineering Department; currently Engineer/Specialist, Aerospatiale Avions, Toulouse, France.

‡Research Assistant, Mechanical and Aerospace Engineering Department.

δ_n = hinge moment correction factor
$\{\theta\}_k$ = parameter vector at time kT_e
λ_k = forgetting factor
μ = mass ratio, $m/(\pi\rho b^2)$
ξ, ξ_0 = nondimensional plunge displacement, h/b, and amplitude, respectively
ρ = air density
$\{\phi\}_k$ = regression vector at time kT_e
ϕ_1, ϕ_2 = phase lag angles for pitch and flap deflection, respectively
$\omega_h, \omega_\alpha, \omega_\beta$ = uncoupled natural frequencies associated with the three degrees of freedom, respectively, $(K_h/m)^{1/2}$, $(K_\alpha/I_\alpha)^{1/2}$, $(K_\beta/I_\beta)^{1/2}$

Subscripts

k = values at time kT_e
T = transpose operator
∞ = freestream values

Introduction

INTERACTION between structural dynamics, aerodynamics, and flight control systems, namely, aeroservoelasticity, has received considerable attention during the last two decades, leading to the development of active control technology (ACT). Extensive research has been carried out on ACT concepts, such as gust alleviation and active flutter suppression. A survey of recent research in this field has been presented by Noll.[1]

Until the last decade, lack of efficient computational tools has restricted the study of aeroservoelastic systems to linear subsonic and supersonic flight regimes. Since then, progress in computational fluid dynamics (CFD) has led to accurate computations of two-dimensional and three-dimensional unsteady transonic aerodynamic loads for viscous and inviscid flows in the time domain. However, inasmuch as numerous simulations based on the direct integration of the aerodynamic equations in the time domain must be performed for aeroservoelastic studies, theoretical aeroelastic studies combining control surfaces with a CFD approach have relied primarily on solution of the transonic small disturbance equation[2–4] and the full potential equation.[5–7]

Guruswamy and Tu[3] pointed out that the combined effect of the shock wave and flow discontinuity due to the presence of the control surface hinge can significantly influence both the aerodynamic and aeroelastic behavior of the wing. Using a simple control law, where the flap deflection angle was proportional to the angle of attack, it was found that at high transonic speeds, when shock waves moved aft of the hinge axis, the active control surface became ineffective, and studies on an F5 wing[4] produced similar results. The importance of simultaneous integration of structures, aerodynamics, and active controls in the transonic domain is clearly emphasized by this concise review.

Recently, aeroelastic studies based on the Euler equations were carried out and efficient computational codes have been developed and applied to the study of two-dimensional and three-dimensional problems.[8–11] The use of Euler equations allowed studies of transonic flows with strong shock waves, where nonlinear phenomena, such as weak divergence and limit cycle flutter, can occur. The role of shock dynamics in transonic flutter was clarified by Bendiksen.[12] In another study, a digital adaptive controller was applied to the active time-varying flight conditions in subsonic and transonic flows.[13,14] The controller was found to be robust and efficient under both random external loads and time-varying conditions. The aerodynamic loads were computed by a crude approximation of the three-dimensional unsteady transonic aerodynamic loads in the time domain, for time-varying freestream Mach numbers.

Another important issue related to aeroservoelastic computation is the need to compare the computational results to experimental data obtained from tests. Such results are often obtained by conducting aeroservoelastic tests on scaled wind-tunnel models built according to aeroelastic scaling laws.[1,15] However, these aeroelastic scaling laws[15] have been developed for simple situations, which do not account for issues such as actuation and control and, therefore, need to be reexamined in the context of more complicated systems encountered in current applications.

This study has several objectives. 1) Model the strong fluid–structure coupling present in transonic flow and determine its influence on control law design, by solving the complete Euler equations about a two-dimensional airfoil trailing-edge control surface combination. 2) Establish the behavior of the aeroservoelastic system in the open-loop mode and study flutter suppression using an adaptive controller that was found to be successful in earlier studies.[13,14] 3) Examine aeroelastic scaling requirements for an aeroservoelastic system, including actuator moment and control power.

The numerical results presented in the paper illustrate interesting aspects of transonic flutter suppression in the presence of aerodynamic nonlinearities and shock waves. Using these results, scaling for aeroservoelastic models can be extracted.

Formulation of the Aeroservoelastic Model and Method of Solution

Aeroservoelastic Model

The aeroelastic model (shown in Fig. 1) consists of a typical cross section of a wing having plunge and pitch degrees of freedom (DOF), combined with a trailing-edge control surface representing an actively controlled flap. In practice, there is a gap between the flap and the airfoil. Correct treatment of the flow in the gap requires the treatment of viscous effects. Because the viscous effects are excluded from this study, the actual physical gap due to the presence of the flap will be eliminated. However, hinge moment corrections will be introduced in an approximate manner to account for this neglect.

The kinetic energy of the three-DOF system has the following form:

$$\bar{T} = \tfrac{1}{2} m b^2 \{\dot{q}\}^T [M] \{\dot{q}\} \tag{1}$$

where

$$\{q\}^T = [\xi \quad \alpha \quad \beta] \tag{2}$$

$$[M] = \begin{bmatrix} 1 & x_\alpha & x_\beta \\ x_\alpha & r_\alpha^2 & r_\beta^2 + x_\beta(c_\beta - a_h) \\ x_\beta & r_\beta^2 + x_\beta(c_\beta - a_h) & r_\beta^2 \end{bmatrix} \tag{3}$$

As in Ref. 15 (Chap. 9), the displacements of the airfoil are restrained by elastic springs: a linear spring located at the elastic axis restrains bending h, a torsional spring located at the same axis restrains pitching α, and the flap rotation β is restrained by a torsional spring at the flap hinge axis. These springs are representative of the structural stiffnesses of the system. Therefore, the strain energy of the three-DOF airfoil section has the following expression:

$$U = \tfrac{1}{2} K_h h^2 + \tfrac{1}{2} K_\alpha \alpha^2 + \tfrac{1}{2} K_\beta \beta^2 \tag{4}$$

A more convenient expression of the strain energy in terms of uncoupled natural frequencies is given by

$$U = \tfrac{1}{2} m b^2 \omega_\alpha^2 \{q\}^T [K] \{q\} \tag{5}$$

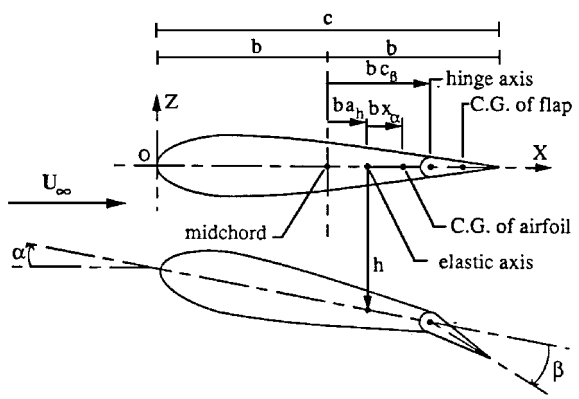

Fig. 1 Definition of parameters for three-DOF aeroservoelastic model.

with

$$[K] = \begin{bmatrix} (\omega_h/\omega_\alpha)^2 & 0 & 0 \\ 0 & r_\alpha^2 & 0 \\ 0 & 0 & (\omega_\beta/\omega_\alpha)^2 r_\beta^2 \end{bmatrix} \tag{6}$$

Neglecting structural damping and using the preceding nondimensional expressions of the kinetic and potential energies together with Lagrange's equations yields the equations of motion for this three-DOF aeroelastic system

$$[M]\{\ddot{q}\} + \omega_\alpha^2[K]\{q\} = \frac{1}{\pi\mu}\bar{U}^2\omega_\alpha^2 \begin{Bmatrix} -C_l \\ 2C_m \\ 2C_h \end{Bmatrix} \tag{7}$$

where the right-hand side of Eq. (7) represents the nondimensional generalized aerodynamic load.

The aerodynamic coefficients are computed by integrating the pressure distribution around the airfoil. Unsteady flow calculations have shown that trailing-edge control surface pressure distribution and hinge moment coefficients are generally overestimated when viscous effects are neglected. Moreover, the gap between the control surface and the wing was not considered in this study. A constant hinge moment correction factor δ_n, based on empirical information, is introduced to correct the hinge moment coefficient in an appropriate manner.

Integration of the Aerodynamic and Structural Equations

The unsteady solution of the Euler equations is based on a finite element approach developed by Bendiksen[16] and Davis and Bendiksen,[17] where aerodynamic and structural equations are written in the same form and thus can be solved simultaneously by the same time-marching algorithm. The spatial discretization of the aerodynamic equations leads to a set of vector equations for the two-dimensional case written for each node i of the mesh:

$$\frac{\mathrm{d}}{\mathrm{d}t}\sum_{j=1}^{N_n}[m]_{ij}\{\boldsymbol{w}_j\} + \{\boldsymbol{Q}_i\} - \{\boldsymbol{D}_i\} = 0 \tag{8}$$

where $[[m]_{ij}]_{i,j=1,Nn}$ and $[\{\boldsymbol{Q}_1\}^T, \ldots, \{\boldsymbol{Q}_{Nn}\}^T]^T$ are the global consistent mass matrix and the global flux vector of the mesh surrounding the airfoil. The quantity $\{\boldsymbol{w}_j\}$ is the vector of flow variables (density, Cartesian momentum components, total energy) at node j, and $\{\boldsymbol{D}_i\}$ is an artificial dissipation term at node i, added so as to damp out numerical oscillations without adding mass, momentum, or energy to the system. Because of the coupling present in the consistent mass matrix, the aerodynamic equations are not in explicit form. To simplify the solution procedure a diagonalized lumped mass matrix $[[m_L]_{ii}]$ is used. The cases studied in Ref. 17 show that the use of the consistent mass formulation did not provide any improvement in accuracy when compared to the lumped mass approach.

The second-order linear differential equation for the aeroservoelastic system [Eq. (7)] is transformed into a first-order state variable equation, similar to Eq. (8),

$$\frac{\mathrm{d}}{\mathrm{d}t}([M_{\mathrm{ST}}]\{\boldsymbol{w}_{\mathrm{ST}}\}) + \omega_\alpha^2[K_{\mathrm{ST}}]\{\boldsymbol{w}_{\mathrm{ST}}\} = \omega_\alpha^2\frac{\bar{U}^2}{\pi\mu}\{R_{\mathrm{ST}}\} \tag{9}$$

where

$$\{\boldsymbol{w}_{\mathrm{ST}}\} = \begin{Bmatrix} \{q\} \\ \{\dot{q}\} \end{Bmatrix} \tag{10}$$

$$[M_{\mathrm{ST}}] = \begin{bmatrix} \omega_\alpha^2[I] & [0] \\ [0] & [M] \end{bmatrix} \tag{11}$$

$$[K_{\mathrm{ST}}] = \begin{bmatrix} [0] & -[I] \\ [K] & [0] \end{bmatrix} \tag{12}$$

$$\{R_{\mathrm{ST}}\} = [0 \quad 0 \quad 0 \quad -C_l \quad 2C_m \quad 2C_h]^T \tag{13}$$

The near-field boundary condition consists of the requirement of flow tangency at the airfoil surface that is implemented through the expressions for the flux terms.[17] In the far field, a characteristic analysis based on Riemann invariants is used to determine the values of the flow variables on the exterior boundary of the mesh. This analysis is described in Refs. 18–21 and was also used in Refs. 22 and 23. It correctly accounts for wave propagation in the far field, which is important for rapid convergence to steady state and serves as a nonreflecting boundary condition for unsteady applications.

A five-stage Runge–Kutta scheme is used to integrate the space-discretized system of the nonlinear equations [Eqs. (8) and (9)] in time. For computational efficiency, the dissipative terms are evaluated only during the first two stages and frozen for the remaining three, as first suggested in Ref. 18. Coefficients for this scheme found to provide good stability characteristics[20] are

$$\alpha_1 = \tfrac{1}{4}, \qquad \alpha_2 = \tfrac{1}{6}, \qquad \alpha_3 = \tfrac{3}{8}, \qquad \alpha_4 = \tfrac{1}{2}, \qquad \alpha_5 = 1 \tag{14}$$

These values were successfully used in Refs. 12, 16, and 17 for both steady and unsteady calculations and, therefore, they are also used in our study.

To maintain mesh accuracy during airfoil motion a boundary fitted dynamic computational mesh algorithm should be capable of conforming continuously to the instantaneous position of the airfoil, while preserving the smoothness of the original mesh. In Ref. 17, the mesh is deformed smoothly from zero at the far-field boundary to the values dictated by the airfoil pitch and plunge motions at the fluid–structure boundary. The node displacements are equal to the displacements computed under the assumption that the mesh is attached to the airfoil as a rigid body, multiplied by time-independent scale factors. These scale factors vary linearly with distance from the airfoil, ranging from unity at the airfoil surface to zero at the outer boundary. This method is quite simple to implement and produces smooth mesh deformations. In this study, presence of a moving flap prevents treatment of the airfoil as a rigid body. Therefore, substantial modifications to the mesh deformation scheme are required to account for the presence of the control surface.

A new modified approach combines the sequential application of two methods. First, the approach given in Ref. 17 is used to compute the position of the nodes as dictated by the instantaneous position in pitch and plunge of the airfoil, with undeflected flap. Then nodes associated with the flap are rotated around the hinge axis by an amount given by the instantaneous flap deflection angle, which produces a substantial deformation of the elements surrounding the flap. Therefore, nodes in this area have to be modified. This is done using a deformation scheme similar to Batina's.[22,23] A submesh surrounding the trailing edge is defined, for which nodes are moved. The submesh used in this study consists of the nodes that are less than half a chord from the trailing edge in the original mesh, where pitch, plunge, and flap displacements are zero. The mesh is modeled as a spring network, where each edge of each cell represents a linear spring. The spring stiffness is taken to be inversely proportional to the original length of the edge. Then the displacements of the submesh nodes are computed by writing the static equilibrium equations at each node and by solving the system using Jacobi or successive overrelaxation (SOR) iterations. The iterations are initialized by the displacement of the submesh nodes at the preceding step (predictor–corrector procedure). Because of the predictor step, only one iteration is required to accurately move the mesh, using SOR iterations.

Implementation of Adaptive Control Laws

This study follows the approach described in Ref. 13, where a single input/single output deterministic autoregressive moving average (ARMA) model, given in Ref. 24, with $2M$ autoregressive (AR) coefficients, $a_i, i = 1, 2, \ldots, 2M$, and $2M$ moving average (MA) coefficients, $b_i = 1, 2, \ldots, 2M$, is used to describe the input–output relation for the aeroservoelastic system:

$$y_k + \sum_{i=1}^{2M} a_i y_{k-i} = \sum_{i=1}^{2M} b_i \beta_{k-i} \tag{15}$$

In vector form

$$y_k = \{\theta\}_k^T \{\phi\}_k \tag{16}$$

where the parameter vector $\{\theta\}_k$ and regression vector $\{\phi\}_k$ are defined as follows:

$$\{\theta\}_k^T = [-a_1 \quad -a_2 \cdots -a_{2M} \quad b_1 \quad b_2 \cdots b_{2M}]$$

$$\{\phi\}_k = [y_{k-1} \quad y_{k-2} \cdots y_{k-2M} \quad \beta_{k-1} \quad \beta_{k-2} \cdots \beta_{k-2M}]$$

where in Eq. (16) y_k are the wing response and control surface deflection angle at a discrete time k, respectively. The input–output description corresponding to Eq. (16) is equivalent to a state-space description, which can be written as

$$\{x_p\}_{k+1} = [A_p]\{x_p\}_k + \{B_p\}\beta_k \tag{17}$$

$$y_k = [C_p]\{x_p\}_k \tag{18}$$

The state vector $\{x_p\}_k$ is defined as

$$\{x_p\}_k = \begin{Bmatrix} y_k \\ h_1(k) \\ \cdots \\ \cdots \\ h_{2M-1}(k) \end{Bmatrix} \tag{19}$$

with

$$\begin{aligned} y_k &= -a_1 y_{k-1} + b_1\beta_{k-1} + h_1(k-1) \\ h_1(k) &= -a_2 y_{k-1} + b_2\beta_{k-1} + h_2(k-1) \\ &\quad - - - - - \\ h_{2M-2}(k) &= -a_{2M-1} y_{k-1} + b_{2M-1}\beta_{k-1} + h_{2M-1}(k-1) \\ h_{2M-1}(k) &= -a_{2M} y_{k-1} + b_{2M}\beta_{k-1} \end{aligned} \tag{20}$$

The state-space description in Eqs. (17) and (18) is in observer form and is completely observable.[25]

The on-line parameter estimation of the AR and MA coefficients in the matrices $[A_p]$ and $[B_p]$ is accomplished using Bierman's U–D (BUD) algorithm,[26] which can be written as

$$\begin{aligned} \{\theta\}_k &= \{\theta\}_{k-1} + \{L\}_k\left(y_k - \{\theta\}_{k-1}^T\{\phi\}_k\right) \\ \{L\}_k &= \frac{[V]_{k-1}\{\phi\}_k}{\lambda_k + \{\phi\}_k[V]_{k-1}\{\phi\}_k} \\ [V]_k &= \frac{[V]_{k-1}}{\lambda_k} - \frac{[V]_{k-1}\{\phi\}_k\{\phi\}_k^T[V]_{k-1}}{\lambda_k\left(\lambda_k + \{\phi\}_k^T[V]_{k-1}\{\phi\}_k\right)} \end{aligned} \tag{21}$$

where $[V]_k$ is the covariance matrix defined as $[V]_k = [U]_k\,[D]_k \times [U]_k^T$. A detailed description of the calculation of the diagonal matrix $[D]_k$ and an upper triangular matrix $[U]_k$, whose diagonal elements are equal to 1, can be found in Ref. 26. The BUD algorithm is a modified version of a recursive least squares algorithm that ensures the positive definiteness of the covariance matrix during estimation. Once the AR and MA coefficients are estimated, the state vector can be calculated using Eq. (20).

The last stage in the implementation of the adaptive controller consists of the on-line control law design, which is described next. The estimated aeroservoelastic system parameters are treated as if they were true, i.e., uncertainties in the estimation are not considered. The adaptive optimal control law is designed to minimize the linear quadratic performance index J

$$J = \sum_{k=0}^{\infty}\left(\{x_p\}_k^T[Q]\{x_p\}_k + r_w\beta_k^2\right) \tag{22}$$

where $[Q]$ is a positive semidefinite symmetric matrix and r_w is a positive constant. It can be shown that the following control law would be optimal[27] for J:

$$\beta_k = -\{G\}_k^T\{x_p\}_k \tag{23}$$

where the controller gain vector $\{G\}_k$ is based on

$$\{G\}_k^T = \frac{\{B_p\}^T[P]_k[A_p]}{r_w + \{B_p\}^T[P]_k\{B_p\}} \tag{24}$$

In the last expression, $[P]_k$ is the Riccati matrix obtained from

$$[P]_k = [A_p]^T\left([P]_{k-1} - \frac{[P]_{k-1}\{B_p\}\{B_p\}^T[P]_{k-1}}{r_w + \{B_p\}^T[P]_{k-1}\{B_p\}}\right)[A_p] + [Q] \tag{25}$$

If the aeroservoelastic system is stabilizable, the Riccati matrix $[P]_k$ will converge to a constant nonnegative symmetric matrix $[P]$, which satisfies the discrete-time algebraic Riccati equation

$$[P] = [A_p]^T\left([P] - \frac{[P]\{B_p\}\{B_p\}^T[P]}{r_w + \{B_p\}^T[P]\{B_p\}}\right)[A_p] + [Q] \tag{26}$$

At time k the Riccati matrix $[P]_k$ in Eq. (25) can be obtained by a fairly simple iterative procedure, which consists of the following steps: 1) calculate $[P]_k$ based on Eq. (25) and 2) if the Riccati matrix $[P]_k$ has converged, proceed to the next step. Otherwise, set $[P]_{k-1} = [P]_k$ and return to step 1.

Only a single iteration is implemented at each discrete time step, so as to reduce the computation time for the control law design procedure.[24] The adaptive optimal control law given in Eq. (23) is obtained by using the estimated aeroservoelastic system matrices $[A_p]$ and $\{B_p\}$ together with a single iteration of Eq. (25). Finally, note that a number of special features of the computer simulation are relevant. These are associated with the learning period, the forgetting factor, and the computational delay. Additional information on these details can be found in Ref. 13.

Aeroelastic Scaling

Aeroelastic scaling laws can be obtained by extending the classical approach presented in Ref. 15 (Chap. 11). Using Eqs. (3), (6), and (7), one has

$$mb^2[M]\{\ddot{q}\} + mb^2\omega_\alpha^2[K]\{q\} = \begin{Bmatrix} -Lb \\ M_\alpha \\ H_\beta \end{Bmatrix} = \rho b^4\bar{U}^2\omega_\alpha^2\begin{Bmatrix} -c_l \\ 2c_m \\ 2c_h \end{Bmatrix} \tag{27}$$

It is useful to obtain first the scaling relations for incompressible flow, under the assumption of simple harmonic motion, and then extend these relations to a more general case. For the incompressible case, the aerodynamic loads can be written as

$$\begin{aligned} \begin{Bmatrix} -Lb \\ M_\alpha \\ H_\beta \end{Bmatrix} &= \rho b^4\begin{bmatrix} -\pi & \pi a_h & T_1 \\ \pi a_h & -\pi\left(\frac{1}{8} + a_h^2\right) & -2T_{13} \\ T_1 & -2T_{13} & T_3/\pi \end{bmatrix}\{\ddot{q}\} \\ &+ \rho b^3 V\begin{bmatrix} 0 & -\pi & +T_4 \\ 0 & -\pi\left(a_h - \frac{1}{2}\right) & -T_{16} \\ 0 & -T_{17} & -T_{19}/\pi \end{bmatrix}\{\dot{q}\} \\ &+ \rho b^2 V^2\begin{bmatrix} 0 & 0 & 0 \\ 0 & 0 & -T_{15} \\ 0 & 0 & -T_{18}/\pi \end{bmatrix}\{q\} + \rho b^2 V^2 C(k) \\ &\times \begin{bmatrix} 0 & -2\pi & -2T_{10} \\ 0 & 2\pi\left(\frac{1}{2} + a_h\right) & 2\left(\frac{1}{2} + a_h\right)T_{10} \\ 0 & -T_{12} & -T_{10}T_{12}/\pi \end{bmatrix}\{q\} + \rho b^3 V C(k) \\ &\times \begin{bmatrix} -2\pi & -2\pi\left(\frac{1}{2} - a_h\right) & -T_{11} \\ 2\pi\left(\frac{1}{2} + a_h\right) & 2\pi\left(\frac{1}{4} - a_h^2\right) & T_{11}\left(\frac{1}{2} + a_h\right) \\ -T_{12} & -T_{12}\left(\frac{1}{2} - a_h\right) & -T_{11}T_{12}/2\pi \end{bmatrix}\{\dot{q}\} \end{aligned} \tag{28}$$

where the nondimensional coefficients T_i are defined in Ref. 28, and they depend only on the nondimensional hinge location c_β. Note that only T_1–T_{14} are independent and the additional T_i represent

convenient combinations of the preceding T_i. The assumption of simple harmonic motion implies

$$\begin{Bmatrix} \xi(t) \\ \alpha(t) \\ \beta(t) \end{Bmatrix} = \begin{Bmatrix} \xi_0 e^{i\omega t} \\ \alpha_0 e^{i\omega t + \phi_1} \\ \beta_0 e^{i\omega t + \phi_2} \end{Bmatrix} \tag{29}$$

where ϕ_1 and ϕ_2 represent phase lag angles. Combining Eqs. (27–29) and dividing by $mb^2\omega^2$,

$$\begin{aligned} &-\xi_0 - x_\alpha \alpha_0 e^{i\phi_1} - x_\beta \beta_0 e^{i\phi_2} + (\omega_\alpha/\omega)^2(\omega_h/\omega_\alpha)^2 \xi_0 \\ &\quad = F_1\left(\mu, a_h, \xi_0, \alpha_0 e^{i\phi_1}, \beta_0 e^{i\phi_2}, c_\beta, k\right) \\ &-x_\alpha \xi_0 - r_\alpha^2 \alpha_0 e^{i\phi_1} - \left[r_\beta^2 + (c_\beta - a_h)x_\beta\right] \cdot \beta_0 e^{i\phi_2} \\ &\quad + r_\alpha^2(\omega_\alpha/\omega)^2 \alpha_0 e^{i\phi_1} = F_2\left(\mu, a_h, k, c_\beta, \xi_0, \alpha_0 e^{i\phi_1}, \beta_0 e^{i\phi_2}\right) \\ &-x_\beta \xi_0 - \left[r_\beta^2 + (c_\beta - a_h)x_\beta\right]\alpha_0 e^{i\phi_1} - r_\beta^2 \beta_0 e^{i\phi_2} \\ &\quad + r_\beta^2(\omega_\alpha/\omega)^2(\omega_\beta/\omega_\alpha)^2 \beta_0 e^{i\phi_2} \\ &\quad = F_3\left(\mu, a_h, k, c_\beta, \xi_0, \alpha_0 e^{i\phi_1}, \beta_0 e^{i\phi_2}\right) \end{aligned} \tag{30}$$

Equations (30) allow one to establish basic aeroelastic scaling relations for the incompressible case. The primary quantities are mass M, length L, and time T. A convenient set of dimensionless quantities governing the problem can be extracted from Eq. (30) and is given by $\xi_0 = h_0/b$, $\omega b/V = k$, $\mu = m/\rho b^2\pi$, $\omega_h/\omega_\alpha = \sqrt{[(K_h/m)/(K_\alpha/I_\alpha)]}$, $\omega_\beta/\omega_\alpha$, ω_α/ω, r_α^2, r_β^2, c_β, a_h, $x_\alpha = S_\alpha/mb$, $x_\beta = S_\beta/mb$, α_0, β_0, ϕ_1, and ϕ_2. There are a total of 16 nondimensional parameters. The first 12 can be expressed as various combinations of the physical quantities that depend on the primary variables M, L, and T, whereas the last 4 are pure nondimensional quantities. When dealing with the aeroelastic stability problem, which is homogeneous, the number of dimensionless ratios can be reduced by one by dividing through by one of the quantities, such as α_0, so as to form a new parameter $h_0/b\alpha_0$; however, this approach would not be useful when dealing with an aeroservoelastic problem. When considering the aeroelastic stability problem, the quantities of interest are $\omega_F b/V_F$, ω_F/ω_α, and $h_0/b\alpha_0$, where the subscript F refers to the value at the flutter condition. To obtain these quantities, the model must have all other nondimensional parameters such as: μ, (ω_h/ω_α), $(\omega_\beta/\omega_\alpha)$, ..., etc., with the correct values. Furthermore, the external shape, i.e., airfoil type, and Reynolds number Re should also be maintained.

The model is subject to only three independent limitations, because these are associated with the three primary quantities. The scaling for the primary quantities can be expressed in general form by

$$L_m/L_w = n_L, \qquad T_m/T_w = n_T, \qquad M_m/M_w = n_M \tag{31}$$

where the subscripts m and w refer to the model and full-scale configuration, respectively. Also note that another nondimensional parameter, namely, the nondimensional velocity $\bar{U} = (V/b\omega_\alpha)$, also plays an important role when dealing with aeroelastic scaling. When compressibility is also considered in the aeroelastic scaling process the list of 16 nondimensional parameters mentioned earlier, has to be augmented by two additional parameters: the Mach number M_∞ and the ratio of specific heats γ. Note that simultaneous scaling of Mach and Reynolds number is virtually impossible unless one uses the full-scale configuration.

The aeroelastic scaling considerations just discussed are based on classical flutter solutions that are obtained from Eqs. (27–30). Most modern aeroelastic studies are based on more refined computer simulations, similar to that used in this study. Such computer solutions[29] can be viewed as similarity solutions of the equations of motion governing the problem[30] and can be combined with the classical approach to obtain more general aeroelastic scaling requirements.

Another facet of aeroelastic scaling manifests itself in the class of problems represented by aeroservoelasticity, where it is important to determine scaling requirements for the hinge moment of the control surface used for flutter suppression, together with the power requirements for the controller inasmuch as these quantities yield important information on the practical implementation of the control system on the full scale vehicle. Consider, first, the hinge moment per unit span

$$H = 2\rho V^2 b^2 C_h$$

and nondimensionalize it as

$$\begin{aligned} \bar{H} = \frac{H}{m\omega^2 b^2} &= \frac{2\rho V^2 b^2}{m\omega^2 b^2} C_h = \frac{2}{\pi}\left(\frac{\pi\rho b^2}{m}\right)\frac{V^2}{\omega^2 b^2} C_h \\ &= \frac{2}{\pi\mu}\frac{1}{k^2} C_h = \frac{2}{\pi}\frac{\bar{U}^2}{\mu}\left(\frac{\omega_\alpha}{\omega}\right)^2 C_h \end{aligned} \tag{32}$$

An important quantity is the instantaneous power per unit span required for control flap actuation given by

$$P(t) = H(t)\dot{\beta}(t)$$

and nondimensional instantaneous power per unit span can be written as

$$\begin{aligned} \bar{P} = \frac{P(t)}{m\omega^3 b^2} &= \frac{2}{\pi}\left(\frac{\pi\rho b^2}{m}\right)\frac{1}{k^2} C_h \frac{\dot{\beta}}{\omega} \\ &= \frac{2}{\pi}\frac{\bar{U}^2}{\mu}\left(\frac{\omega_\alpha}{\omega}\right)^2 C_h \frac{\dot{\beta}}{\omega} = \frac{2}{\pi}\frac{\bar{U}^2}{\mu}\left(\frac{\omega_\alpha}{\omega}\right)^3 C_h \frac{\dot{\beta}}{\omega_\alpha} \end{aligned} \tag{33}$$

For certain applications, instantaneous power can be misleading and, therefore, it is also useful to define an average power; such a quantity, however, will be application dependent:

$$\bar{P}_{\text{av}} = \frac{2}{\pi}\frac{\bar{U}^2}{\mu}\left(\frac{\omega_\alpha}{\omega}\right)^3 \frac{1}{\bar{t}_2 - \bar{t}_1}\int_{\bar{t}_1}^{\bar{t}_2} C_h(\bar{t})\frac{\dot{\beta}(\bar{t})}{\omega_\alpha}\,\mathrm{d}\bar{t} \tag{34}$$

The average power per unit span, given by Eq. (34), is the average power in a nondimensional time period $(\bar{t}_2 - \bar{t}_1)$, during which the pitch angle response is reduced by 50% from its initial value. Equations (32–34) have interesting implications when considering aeroservoelastic testing of aeroelastically scaled models and the application of these results to a full-scale configuration.

Results and Discussion

Calculations presented were carried out for NACA 0012 and NACA 64A006 airfoils, using grids derived from a structured quadrilateral cell O mesh. Both mesh configurations consisted of 4092 node points of which 126 were on the airfoil surface and 128 were on the far-field boundary, which is located at a radius of 25 chords. A partial view of the NACA 0012 mesh in the deformed state, for a nose-up pitch angle of 10 deg, a plunge displacement of $-0.02b$, and a positive flap deflection angle of 10 deg is shown in Fig. 2. Before undertaking the control studies the computer code was carefully validated by comparing the results obtained for a number of cases with those obtained in Refs. 17, 31, and 32. These correlation studies were described in Ref. 29.

Open-Loop Studies

Two typical section wing models are considered. The first model is the NACA 64A006 typical section considered in Ref. 33 and in Refs. 9, 12, and 16, which is described by the following nondimensional parameters when using our notation:

$$a_h = -0.2, \qquad x_\alpha = 0.2$$

$$r_\alpha \simeq 0.5385, \qquad \omega_h/\omega_\alpha = 0.3434$$

The second example is the NACA 0012 benchmark model, tested experimentally at the NASA Langley Research Center[34] and studied

in Ref. 12. The nondimensional parameter values describing this configuration are

$$a_h = 0.0, \qquad x_\alpha = 0.0, \qquad r_\alpha^2 = 0.25, \qquad \omega_h/\omega_\alpha = 0.6564$$

For both models, calculations were performed at several values of Mach number, mass ratio μ, and nondimensional speeds $\bar{U}$. Such results were computed for $x_\beta = 0.008, r_\beta = 0.06$, and $\omega_\beta/\omega_\alpha = 1.5$ and can be found in Ref. 29. Results obtained were found to be similar to those described in Refs. 8, 9, and 12. Results for the transonic bucket with the flap were also calculated in Ref. 29, and the influence of the flap on the stability boundary was found to be minor.

Active Control Studies

Flutter suppression in transonic flow, using the adaptive controller, was studied for both the NACA 0012 and NACA 64A006 airfoils. As in Ref. 13, $[Q]$ is chosen as the identity matrix. In this study, the output is the vertical acceleration y_k, which is nondimensionalized by multiplying it by a scaling factor $(100 \cdot c\gamma/a_\infty^2)$, and subsequently, it is filtered by a 10-order sine-Butterworth filter. With this definition of y_k, a weighting coefficient, $r_w = 0.01\,(1/\text{rad}^2)$, was found to produce good results.

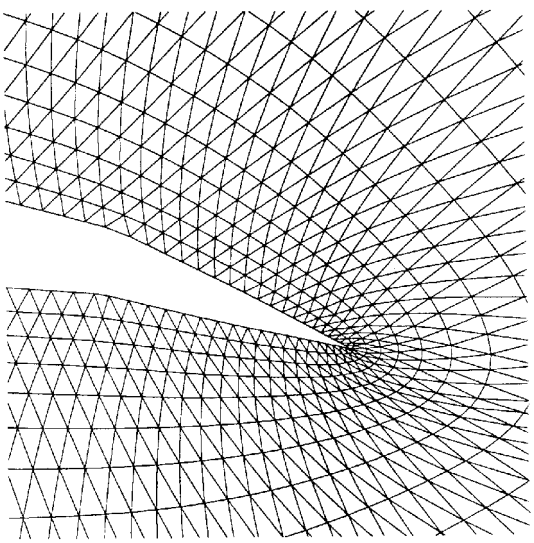

Fig. 2 Partial view of undeformed grid about NACA 0012 airfoil: α = 10 deg, $h = -0.02b$, and β = 10 deg. Mesh for airfoil section: NACA 0012; $X_{\min} = 0.650$, $X_{\max} = 1.150$, $Y_{\min} = -0.250$, and $Y_{\max} = 0.250$.

A typical computer simulation of the aeroservoelastic system contains three important time periods. The first 24 sampling steps constitute the learning period. During this period the control surface is activated randomly to get the initial estimates of the aeroservoelastic system matrices. The maximum amplitude of random control surface deflection angle is limited to 0.8 deg. At the end of the learning period the controller is engaged and the initial condition for the Riccati matrix is obtained using Potter's method.[35] In the second period the active flutter suppression system controls the acceleration at the sensor position, caused by the random control surface motion in the learning period. When the acceleration has been significantly reduced, typically after 48 sampling steps, a perturbation in the angle of attack, the plunge displacement, or plunge and pitch velocities is introduced. In the third period the active flutter suppression system controls the acceleration at the sensor position, caused by this perturbation.

To test the effectiveness of the adaptive controller a step-function perturbation plunge velocity equal to $-0.01b\omega_\alpha\,(= -0.01Ma_\infty/\bar{U})$ is introduced at the end of the second period. This nondimensional value was chosen because at $M = 0.85$, $\bar{U} = 3.0$, and $a_\infty = 1100$ ft/s, it is equal to a vertical velocity change of approximately 3.125 ft/s. Note that the sensor location for the control studies conducted on the NACA 64A006 airfoil was at 50% of the chord, and for the NACA 0012 airfoil studies the sensor location was 60% of chord.

Interaction between maximum flap deflection amplitude, deflection rate, and sampling time step was studied first. The NACA 64A006 airfoil, for which the flutter boundary was plotted in Fig. 3, was considered first. At $M = 0.85$, $\bar{U} = 3.0$ is about 20% higher than the flutter velocity. For this unstable flight condition, simulations were carried out using a flap deflection rate $\mathrm{d}\beta/\mathrm{d}t$ equal to 1.0 deg $a_\infty/(c\sqrt{\gamma})$; thus, with a chord of 10 ft and a freestream speed of sound of 1100 ft/s, where $Te_1 \simeq 0.020$ s, one has $\mathrm{d}\beta/\mathrm{d}t \simeq 93$ deg/s. A sampling time step, $Te_1 = 0.4\pi/\omega_\alpha$, was considered first. When using the maximum flap deflection $\beta_{\max}$ equal to 4 deg, the active controller failed to suppress flutter, as shown in Fig. 3. However, when $\beta_{\max}$ is reduced to 2 deg, the controller successfully suppressed flutter, as shown in Fig. 4. This implies that the failure of the controller in Fig. 3 can be attributed to the inability of the actuator to track the variations of the optimal flap deflection angle around the undeflected position. Indeed, the maximum flap deflection angle variation that the actuator model used in this study is capable of providing during Te_1 is equal to 1.87 deg. Therefore, at a particular sampling time, when the optimal flap deflection angle is negative and

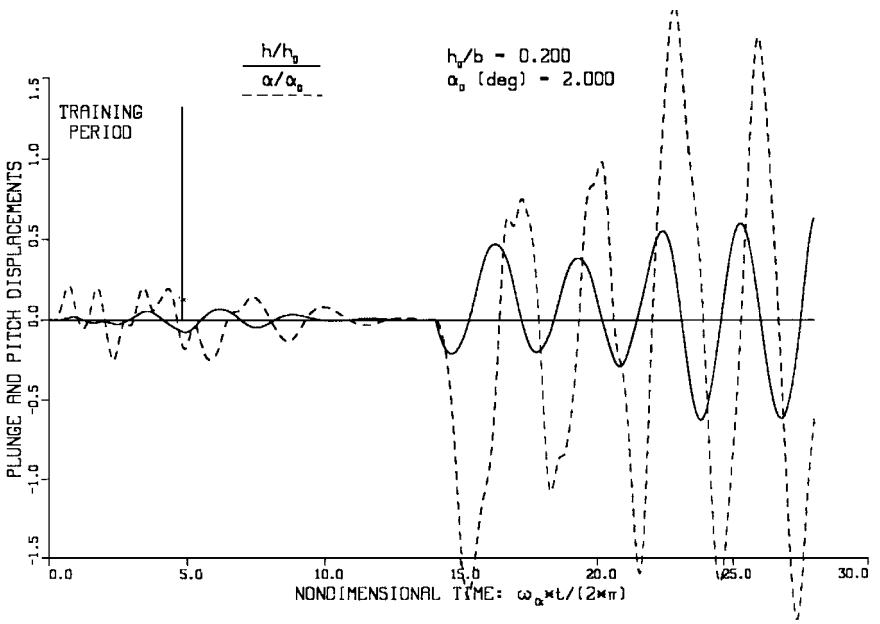

Fig. 3 Time response of the aeroservoelastic system during active flutter suppression with sampling rate $Te = 0.4\pi/\omega_\alpha$ for NACA 64A006 airfoil, with $M = 0.85$, $\bar{U} = 3.0$ (20% above flutter velocity), and $\beta_{\max} = 4$ deg.

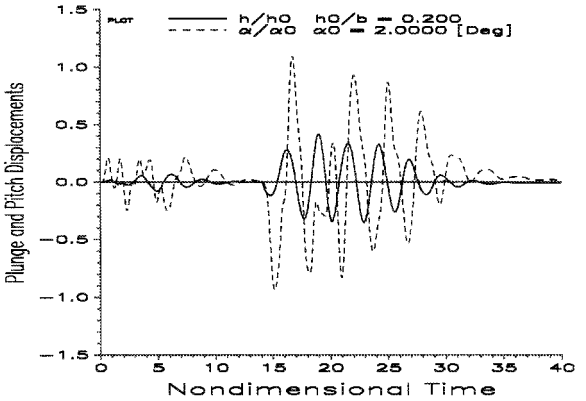

Fig. 4 Time response of the aeroservoelastic system during active flutter suppression with the same conditions as Fig. 3 for NACA 64A006, except $\beta_{max} = 2$ deg.

the current flap deflection angle is 4 deg, then at the next sampling time step, the flap deflection angle will be equal to 2.13 deg, which is far from the desired optimal value. Increasing the sampling time by a factor of two provides the controller with additional time needed to move the flap to its optimal position, and the active controller could suppress flutter even with $\beta_{max} = 4$ deg, as shown in Fig. 5. These results indicate that controller effectiveness is very sensitive to the ability of the actuator to track variations of the optimal flap deflection angle around the undeflected position.

Effects of shock wave and flow discontinuity due to the presence of the hinge were studied next, using the NACA 0012 airfoil. At $M = 0.85$, $\bar{U} = 4.0$ and $\mu = 75.0$, a flutter suppression simulation using $Te_1 = 0.4\pi/\omega_\alpha$, $d\beta/dt = 1.0$ deg $\alpha_\infty/(c\sqrt{\gamma})$, and $\beta_{max} = 2$ deg. It can be seen from Fig. 6 that the active controller was successful in suppressing flutter, despite shock wave oscillations back and forth about the hinge line. The effectiveness of the flap was studied in two different ways: first, by reducing its size and second, by using hinge moment correction factors between 0 and 1. Figure 7 shows the time response of the NACA 0012 airfoil with

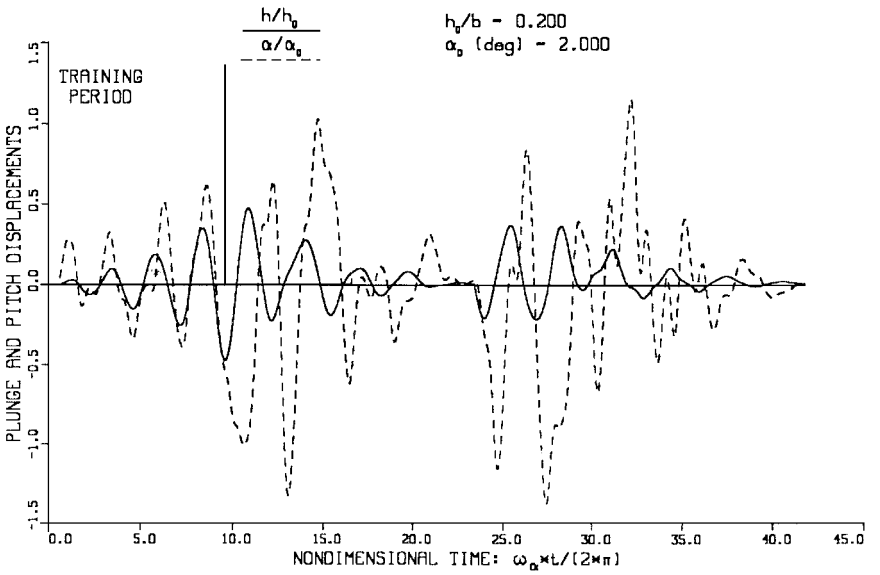

Fig. 5 Time response of the aeroservoelastic system during active flutter suppression with conditions the same as Fig. 3 for NACA 64A006, except the sampling rate is $Te = 0.8\pi/\omega_\alpha$.

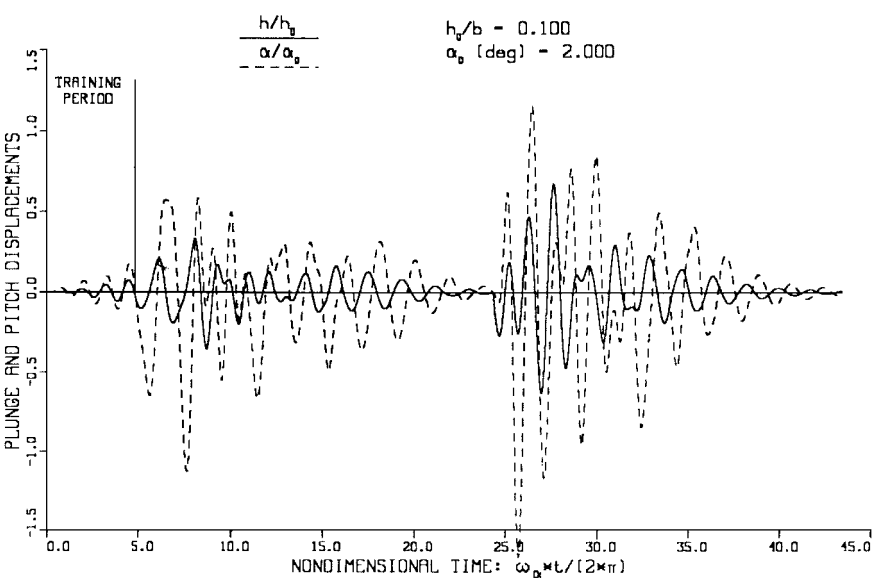

Fig. 6 Time response of the aeroservoelastic system during active flutter suppression for the NACA 0012 airfoil with hinge axis at 75% of chord and $M = 0.85$, $\bar{U} = 4.0$, and $\mu = 75.0$ (20% above the flutter).

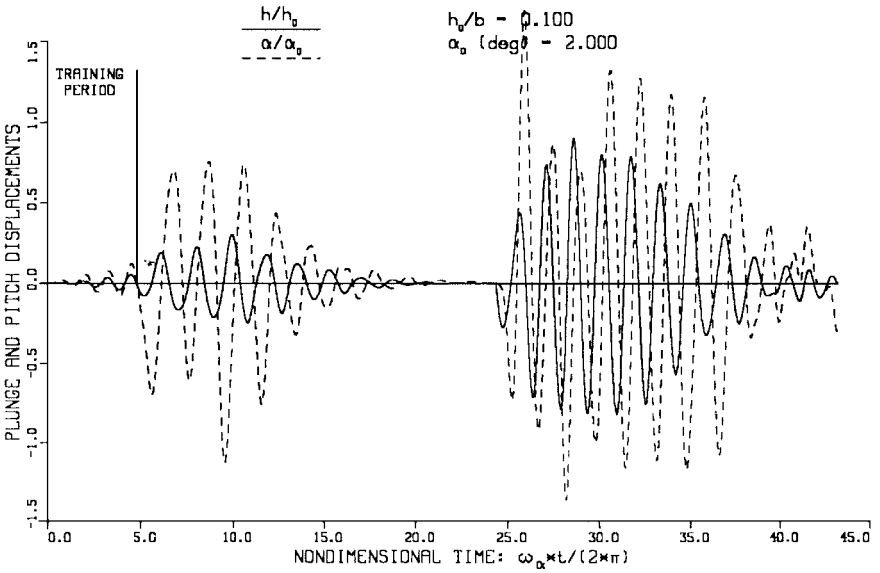

Fig. 7 Time response of the aeroservoelastic system during active flutter suppression for the NACA 0012 airfoil with hinge axis at 85% of chord and all other parameters identical to Fig. 6.

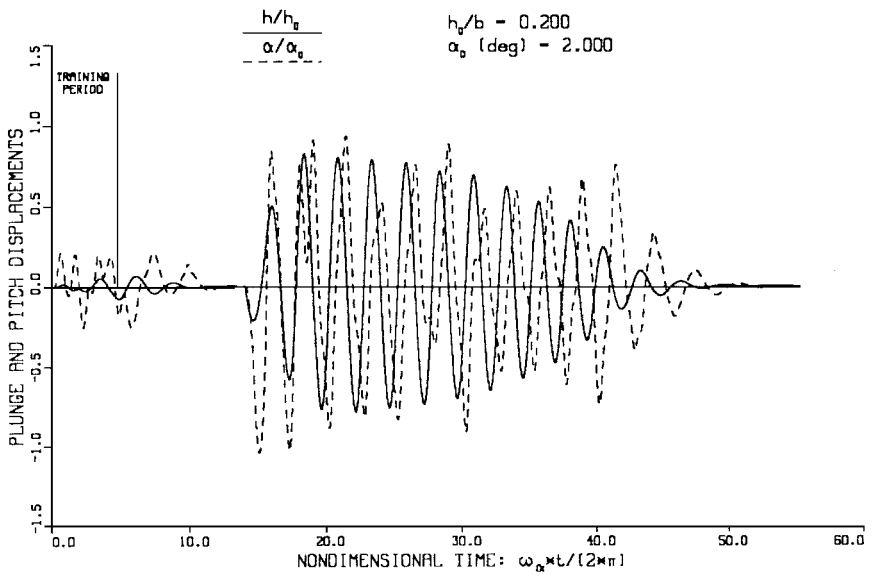

Fig. 8 Effect of hinge moment correction factor on time response of the aeroservoelastic system during active flutter suppression on the 64A006 airfoil, with $\delta_n = 0.75$, $Te = 0.4\pi/\omega_\alpha$, and $\beta_{\max} = 2.0$ deg; all other parameters are identical to Fig. 4.

the same parameters as those used to compute the time response shown in Fig. 6, except for the hinge axis location, which is moved from 75 to 85% of the chord. Figure 8 shows the time response of the NACA 64A006 airfoil with the same parameters as those for Fig. 7, except for the hinge correction factor, which was reduced to 0.75 from 1. Both figures show an increase in the time required to suppress flutter.

Among the cases considered for flutter suppression in transonic flow, the NACA 64A006 airfoil represents a more realistic configuration than the NACA 0012. Therefore, it is interesting to examine the case shown in Fig. 4 and to determine hinge moments and power requirements for flutter suppression. For this particular case, the hinge moment coefficient $C_h(\bar{t})$ is plotted in Fig. 9. The power coefficient given by $C_h(\bar{t})(\mathrm{d}\beta/\mathrm{d}\bar{t})$ is shown in Fig. 10. When operating at sea level conditions and using a 10-ft chord, the instantaneous power per unit span at $\bar{t} = 21$ is $P = 0.20$ hp/ft, and the average power computed between $\bar{t}_1 = 16.6$ and $\bar{t}_2 = 28$ is $P_{\mathrm{av}} = 0.164$ hp/ft. This indicates that fairly modest amounts of power are required for flutter suppression. Using Eqs. (33) and (34), hinge moments and power requirements for other configurations that are aeroelastically similar can be obtained. Note that for some applications one would use only the positive part of the power in Fig. 10.

Another interesting question related to the present study is the scaling of actuators used when implementing active flutter suppression. Recent studies on flutter suppression have emphasized the potential for using piezoelectric actuation for its implementation[36,37]; therefore, it is useful to examine the conclusions obtained in these studies within the framework of aeroelastic scaling considerations. References 36 and 37 describe innovative and pioneering research aimed at demonstrating the use of piezoelectrics for flutter suppression. The actively controlled wing described in these studies uses piezoelectrics bonded to the top and bottom surfaces of a composite sandwich structure, with 2% thickness to chord ratio, which represents the primary load carrying element of the wing model. Details of the wing structure, modal information, flutter velocities, and frequencies are given in Ref. 36. The wing is surrounded by a shell representing a NACA 66-012 airfoil. It has a 30-deg quarter-chord sweep, a span of 48 in., half-span aspect ratio of 4.0, a weight of 11.4 lb, and an approximate chord of 15.6 in. Also note that Ref. 37 clearly states that aeroelastic scaling considerations were not used when designing this wing model, which implies that the model is not aeroelastically scaled. However, it is instructive to apply the aeroelastic scaling relations presented in this paper and see what type of full-scale configuration would correspond to this model. In

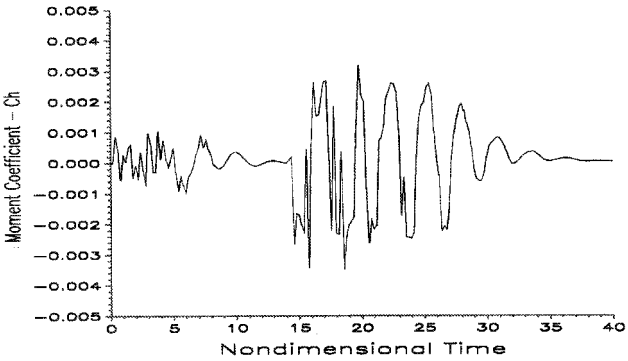

Fig. 9 Hinge moment coefficient during flutter suppression for the case given in Fig. 4.

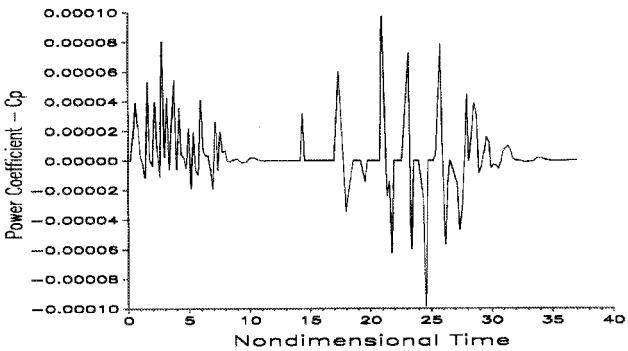

Fig. 10 Power coefficient per unit length during flutter suppression for the case given in Fig. 4.

these calculations, one should keep in mind that there are different ways to find these relations and these calculations represent possible configurations. Assume that $L_m/L_w = \frac{1}{6}$ and $\bar{U}_m = \bar{U}_w$; then

$$\frac{\omega_{\alpha w}}{\omega_{\alpha m}} = \frac{b_m}{b_w}\frac{V_w}{V_m} = \frac{L_m}{L_w}\left(\frac{V_w}{V_m}\right)$$

and from Ref. 37, $\omega_{\alpha m} = 12.4$ Hz and $\omega_{hm} = 2.4$ Hz. Therefore, one has $\omega_{\alpha w} = \omega_{\alpha m}(L_m/L_W) = 12.4/6 = 2.06$ Hz, and for $V_w = 2V_m$, one has $\omega_{\alpha w} = \omega_{\alpha m}/3 = 4.12$ Hz. Thus, both configurations represent wings that are torsionally very soft and, therefore, are relatively easy to control using strain actuation based on piezoelectrics. Similar conclusions can be reached by requiring similarity of reduced flutter frequencies. In the tests $\omega_F \cong 6.1$ Hz, which would correspond to flutter frequencies of 1 Hz when $V_{Fm} = V_{Fw}$, and $\omega_F = 2$ Hz, when $V_{Fw} = 2V_{Fm}$. Using aeroelastic scaling, it can also be shown that $M_w = (L_w/L_n)^3 M_m = 216\,M_m$. The weight of the wing used in the tests was 11.4 lb; this would imply that the weight of the full-scale configuration could be $W_w = 11.4(216) = 2461$ lb, which seems to be quite high. These results show that it is important to conduct tests such as those described in Refs. 36 and 37 on aeroelastically scaled models; otherwise the implication of such results for realistic airplane configuration becomes difficult and confusing.

Concluding Remarks

A two-dimensional aeroservoelastic model consisting of a two-DOF airfoil with a trailing-edge control surface was studied. This model, which is based on exact inviscid aerodynamics, can represent correctly large amplitude motions and the associated strong shock dynamics and, thus, is a good candidate for flutter suppression studies. The adaptive controller was found to be successful for the nonlinear aeroelastic flutter suppression problem, when the actuator was able to track variations of the flap deflection angle around the undeflected position. In the simulations performed, the adaptive controller effectiveness was found to be robust with respect to changes in the hinge moment correction factor and the hinge axis location. This study indicates that implementation of an active flutter suppression systems in the transonic regime requires an integrated approach in which CFD-based loads are used as the basis for the control law design.

Aeroelastic scaling requirements for an actively controlled wing were derived. Such scaling rules can be used together with our computer simulation to establish more complicated scaling requirements between the model and the full-scale configurations. Scaling relations for hinge moment and power required for flutter suppression were also presented, and these relations are valid as long as the same nondimensional time scale is used in the simulation. Finally, it was shown that aeroelastic scaling requirements play a useful role when interpreting experimental results obtained in aeroservoelastic testing.

Acknowledgments

This research was funded by the Air Force Office of Scientific Research Directorate of Aerospace Sciences and Materials under Grant F49620-94-1-0400, with Brian Sanders as Grant Monitor.

References

[1]Noll, T. E., "Aeroservoelasticity," *Flight-Vehicle Materials, Structures, and Dynamics—Assessment and Future Direction*, edited by A. K. Noor and S. L. Venneri, Vol. 5, Structural Dynamics and Aeroelasticity, American Society of Mechanical Engineers, New York, 1993, pp. 179–212.

[2]Yang, T. Y., and Chen, C. H., "Transonic Flutter and Response Analyses of Two Three Degree-of-Freedom Airfoils," *Journal of Aircraft*, Vol. 19, No. 10, 1982, pp. 682–684.

[3]Guruswamy, G. P., and Tu, E. L., "Transonic Aeroelasticity of Fighter Wings with Active Control Surfaces," *Journal of Aircraft*, Vol. 26, No. 7, 1989, pp. 682–684.

[4]Guruswamy, G. P., "Integrated Approach for Active Coupling of Structures and Fluids," *AIAA Journal*, Vol. 27, No. 6, 1989, pp. 788–793.

[5]Isogai, K., "The Development of Unsteady Transonic 3-D Full Potential Code and Its Aeroelastic Applications," *Transonic Unsteady Aerodynamics and Its Aeroelastic Applications*, Paper 17, AGARD Conf. Proceedings No. 374, 1984, pp. 17.1–17.25.

[6]Ide, H., and Shankar, V. J., "Unsteady Full Potential Aeroelastic Computations for Flexible Configurations," AIAA Paper 87-1238, June 1987.

[7]Ide, H., and Ominsky, D., "Simulation of Static and Dynamic Behavior of a Flexible Wing with Multiple Control Surfaces," *Proceedings of the AIAA/ASME/ASCE/AHS/ASC 31st Structures, Structural Dynamics, and Materials Conference* (Long Beach, CA), AIAA, Washington, DC, 1990, pp. 1582–1588 (AIAA Paper 90-1075).

[8]Bendiksen, O. O., and Kousen, K. A., "Transonic Flutter Analysis Using the Euler Equations," AIAA Paper 87-0911, April 1987.

[9]Kousen, K. A., and Bendiksen, O. O., "Nonlinear Aspects of the Transonic Aeroelastic Stability Problem," *Proceedings of the AIAA/ASME/ASCE/AHS/ASC 29th Structures, Structural Dynamics, and Materials Conference* (Williamsburg, VA), AIAA, Washington, DC, 1988, pp. 760–769 (AIAA Paper 87-2306).

[10]Guruswamy, G. P., "Time-Accurate Unsteady Aerodynamic and Aeroelastic Calculations of Wing Using Euler Equations," *Proceedings of the AIAA/ASME/ASCE/AHS/ASC 29th Structures, Structural Dynamics, and Materials Conference* (Williamsburg, VA), AIAA, Washington, DC, 1988 (AIAA Paper 88-2281).

[11]Robinson, B. A., Batina, J. T., and Yang, H. T., "Aeroelastic Analysis of Wings Using the Euler Equations with a Deforming Mesh," *Proceedings of the AIAA/ASME/ASCE/AHS/ASC 31st Structures, Structural Dynamics, and Materials Conference* (Long Beach, CA), AIAA, Washington, DC, 1990, pp. 1510–1518 (AIAA Paper 90-1032).

[12]Bendiksen, O. O., "Role of Shock Dynamics in Transonic Flutter," *Proceedings of the AIAA/ASME/AHS/ASC 33rd Structures, Structural Dynamics, and Materials Conference* (Dallas, TX), AIAA, Washington, DC, 1992, pp. 401–414 (AIAA Paper 92-2121).

[13]Pak, C.-G., Friedmann, P., and Livne, E., "Transonic Adaptive Flutter Suppression Using Approximate Unsteady Time Domain Aerodynamics," *Proceedings of the AIAA/ASME/AHS/ASC 32nd Structures, Structural Dynamics, and Materials Conference* (Baltimore, MD), AIAA, Washington, DC, 1991, pp. 1832–1854 (AIAA Paper 91-0986).

[14]Pak, C., Friedmann, P. P., and Livne, E., "Digital Adaptive Flutter Suppression and Simulation Using Approximate Transonic Aerodynamics," *Journal of Vibration and Control*, Vol. 1, No. 4, 1995, pp. 363–388.

[15]Bisplinghoff, R. L., Ashley, H., and Halfman, R., *Aeroelasticity*, Addison–Wesley, Reading, MA, 1995, Chap. 11.

[16]Bendiksen, O. O., "A New Approach to Computational Aeroelasticity," *Proceedings of the AIAA/ASME/AHS/ASC 32nd Structures, Structural Dynamics, and Materials Conference* (Baltimore, MD), AIAA, Washington, DC, 1991, pp. 1712–1727 (AIAA Paper 91-0939).

[17]Davis, G., and Bendiksen, O. O., "Unsteady Transonic Euler Equations Using Finite Elements," *Proceedings of the AIAA/ASME/AHS/ASC 33rd Structures, Structural Dynamics, and Materials Conference* (Dallas, TX), AIAA, Washington, DC, 1992, pp. 2203–2213 (AIAA Paper 92-2504).

[18]Jameson, A., Schmidt, W., and Turkel, E., "Numerical Solutions of the Euler Equations by Finite Volume Methods Using Runge–Kutta Time Stepping Schemes," AIAA Paper 81-1259, June 1981.

[19]Jameson, A., and Baker, T. J., "Solution of the Euler Equations for Complex Configurations," *Proceedings of the AIAA 6th Computational Fluid Dynamics Conference*, AIAA, New York, 1983, pp. 293–302.

[20]Jameson, A., and Schmidt, W., "Some Recent Developments in Numerical Methods for Transonic Flows," *Computer Methods in Applied Mechanics and Engineering*, Vol. 51, No. 1–3, 1985, pp. 467–493.

[21]Jameson, A., and Mavriplis, D., "Finite Volume Solution of the Two-Dimensional Euler Equations on a Regular Triangular Mesh," *AIAA Journal*, Vol. 24, No. 4, 1986, pp. 611–618.

[22]Batina, J. T., "Unsteady Euler Algorithm with Unstructured Dynamic Mesh for Complex Aircraft Aeroelastic Analysis," *Proceedings of the AIAA/ASME/AHS/ASC 30th Structures, Structural Dynamics, and Materials Conference*, AIAA, Washington, DC, 1989, pp. 275–284 (AIAA Paper 89-1189).

[23]Batina, J. T., "Unsteady Euler Airfoil Solutions Using Unstructured Dynamic Meshes," *AIAA Journal*, Vol. 28, No. 8, 1990, pp. 1381–1388.

[24]Aström, K. R., and Wittenmark, B., *Adaptive Control*, 2nd ed., Addison–Wesley, Reading, MA, 1995, Chaps. 2 and 4.

[25]Goodwin, G. C., and Sin, K. S., *Adaptive Filtering Prediction and Control*, Prentice–Hall, Englewood Cliffs, NJ, 1986, Chap. 2.

[26]Ljung, L., and Söderstrom, T., *Theory and Practice of Recursive Identification*, MIT Press, Cambridge, MA, 1987.

[27]Kim, S. M., "Adaptive LQ Tracking of MIMO Systems and Its Application to Robotic Manipulators with Flexible Joints," Ph.D. Dissertation, Mechanical, Aerospace, and Nuclear Engineering Dept., Univ. of California, Los Angeles, CA, June 1990.

[28]Theodorsen, T., and Garrick. I. E., "Nonstationary Flow About a Wing-Aileron-Tab Combination Including Aerodynamic Balance," NACA TR 736, May 1942.

[29]Guillot, D., and Friedmann, P. P., "A Fundamental Aeroservoelastic Study Combining Unsteady CFD with Adaptive Control," *Proceedings of the AIAA Dynamics Specialists Conference* (Hilton Head, SC), AIAA, Washington, DC, 1994, pp. 385–401 (AIAA Paper 94-1721).

[30]Baker, W. K., Westine, P. S., and Dodge, F. T., *Similarity Methods in Engineering Dynamics*, rev. ed., Elsevier, New York, 1991, Chap. 3.

[31]Magnus, R., and Yoshihara, H., "The Transonic Oscillating Flap," AIAA Paper 76-327, July 1976.

[32]Ballhaus, W., and Goorjian, P., "Implicit Finite-Difference Computations of Unsteady Transonic Flows About Airfoils," *AIAA Journal*, Vol. 15, No. 12, 1977, pp. 1728–1735.

[33]Ashley, H., "Role of Shocks in the Subtransonic Flutter Phenomenon," *Journal of Aircraft*, Vol. 17, No. 3, 1980, pp. 187–197.

[34]Rivera, J. A., Dansberry, B. E., Farmer, M. G., Eckstrom, C. Y., Seidel, D. A., and Bennett, R. M., "Experimental Flutter Boundaries with Unsteady Pressure Distribution for the NACA 0012 Benchmark Model," *Proceedings of the AIAA/ASME/AHS/ASC 32nd Structures, Structural Dynamics, and Materials Conference* (Baltimore, MD), AIAA, Washington, DC, 1991, pp. 1898–1908 (AIAA Paper 91-1010).

[35]Potter, J. E., "Matrix Quadratic Solutions," *SIAM Journal of Applied Mathematics*, Vol. 14, No. 3, 1966, pp. 496–501.

[36]Reich, G. W., vanSchoor, M. C., Lin, C. Y., and Crawley, E. F., "An Active Aeroelastic Wing Model for Vibration and Flutter Suppression," *Proceedings of AIAA/ASME/ASCE/AHS/ASC 36th Structures, Structural Dynamics, and Materials Conference* (New Orleans, LA), AIAA, Washington, DC, 1995, pp. 314–324 (AIAA Paper 95-1193).

[37]Lin, C. Y., Crawley, E. F., and Heeg, J., "Open- and Closed-Loop Results of a Strain-Actuated Active Aeroelastic Wing," *Journal of Aircraft*, Vol. 33, No. 5, 1996, pp. 987–994.